Hindawi Publishing Corporation
International Journal of Rotating Machinery
Volume 2013, Article ID 683713, 11 pages
http://dx.doi.org/10.1155/2013/683713

Research Article

A New Proposed Return Guide Vane for Compact Multistage Centrifugal Pumps

Qihua Zhang,[1] Weidong Shi,[1] Yan Xu,[1] Xiongfa Gao,[1] Chuan Wang,[1] Weigang Lu,[1] and Dongqi Ma[2]

[1] *National Research Center of Pumps and Pumping System Engineering and Technology, Jiangsu University, Zhenjiang 212013, China*
[2] *Fujian Academy of Mechanical Sciences, Fuzhou, Fujian 350005, China*

Correspondence should be addressed to Qihua Zhang; qihua05@163.com

Received 5 April 2013; Accepted 18 July 2013

Academic Editor: J.-C. Han

For widely used multistage centrifugal pumps, their former structures are so bulky that nowadays growing interest has been shifted to the development of more compact structures. Following this trend, a compact pump structure is provided and analysed. To maintain the pump's pressure recovery, as well as to meet the water flow from the impeller, a circumferential twisted return guide vane (RGV) is proposed. To validate this design method, the instantaneous CFD simulations are performed to investigate the rotor-stator interventions. Within the impeller, the pressure fluctuation is cyclic symmetry, where the impeller frequency dominates. At the zone where flow leaves impeller for RGV, the pressure fluctuation is nonperiodic, the impeller frequency is major, and the rotation frequency is secondary. Within RGV, the periodic symmetric fluctuation is recovered, where the rotation frequency is governing. The fluctuation decreases from seven cycles within impeller to two cycles within RGV, indicating that the flow from impeller is well handled by RGV. To examine the pump's performance, a prototype multistage pump is designed. The testing shows that the pump efficiency is 57.5%, and the stage head is 9 m, which is comparable to former multistage centrifugal pumps. And this design is more advantageous in developing compact multistage centrifugal pumps.

1. Introduction

To meet variable flow angles into gas turbines, hydraulic runners, and so forth, inlet guide vane (IGV) is adopted to keep them operating at peak performance [1–5]. For compressors, fans, pumps, and so forth, IGV is also used to manipulate their operating load [6–11]. Outlet guide vane (OGV) is heavily used at downstream of low pressure turbines, fans, compressors, and pumps, where the rotating velocity can be effectively transformed to static pressure, reducing flow-induced vibration and noise [12–19]. Nozzle guide vane (NGV) is widely used in turbines. More specially, return guide vane (RGV) is applied for multistage centrifugal turbomachines, where RGV is functioned as an OGV with respect to its upstream stage; meanwhile, it is served as an IGV with respect to its downstream stage, which increases its design complexity [20–23].

In the first place, a suitable guide vane design is critical for overall stage performance. For IGV and OGV, flow in a mainstream direction is concerned, so airfoil is widely adopted in the streamwise direction, while in the spanwise direction, such strategies as free-vortex method, forced-vortex method, and radial-equilibrium method are available. To improve the performance of an impulse turbine, a free-vortex method was used to design a 3D IGV [1, 2], which achieved a 4.5% efficiency growth. And through a dual-curvature shape technique, an IGV of minihydraulic bulb turbines was proposed, which was validated by prototype turbine tests [3].

In early times, experimental testings were conducted to determine the effects of guide vanes on pump performance. And through comparisons of four guide vane arrangements in terms of pressure head, efficiency, and velocity distributions, it was concluded that RGV played a more crucial role in their multistage pump [20]. With technology advancement, especially with increasing CFD involvement since the 1980s, optimization has been popular in contemporary turbomachine design [24]. And especially for multistage

turbomachines, the focus is the interaction between the rotor and the stator [25]. And sliding mesh technique was used to examine different flow patterns within a multistage pump by [26]. Moreover, rotor-stator interactions were investigated to aid in their design optimizations. By using a rotor-stator shear system, the drop size distribution of emulsification is numerically examined, and it was found that the effective equilibrium drop size was dominated by the rotor shape and its rotating speed [27]. Different combinations of flat type blade and curved-type blade in turbomolecular pumps were numerically investigated with DSMC, and the flat-curved rotor-stator combination was found to be more efficient [28]. The effect of the guide plate on the cavitation erosion on the bottom surface of the guide vane in three Gorges turbine was numerically investigated, and a new vortex structure clarifying this erosion was identified by the numerical simulation, which would be used to design antierosion guide plates [29].

On the other hand, optimal strategy research plays an important role in the turbomachine optimization design. A multiobjective method was performed to optimize a helico-axial pump impeller shape [30]. Monitoring and controlling strategy is an alternative procedure which can be calibrated to manage energy consumption of overall turbomachine systems. Commonly, this is an interdisciplinary and interdepartmental task. And a wide range of statistical investigations were performed upon a large number of pumps in plants to pursue energy saving [31]. And some monitoring techniques have been developed to improve existing pumping system efficiency [32].

Though multistage centrifugal pumps are not so widely applied as turbines, fans, they are indispensable in the deep well water and oil pumping and occupy a considerable market share of household water supply, rural drainage, and urban water circulation. So light weight and mobility are the most important factors concerned by the customers, challenging the former structure of multistage centrifugal pumps [33]. In this study, the difference between former pump structure and compact pump structure is firstly analyzed. And the merit of compact structure is addressed. Then, a new RGV design is proposed to match this compact structure. And the instantaneous rotor-stator interactions are conducted to evaluate RGV performance. Finally, a prototype multistage centrifugal pump is designed and tested to validate the design strategy.

2. RGV Structure Study

Due to inertia, fluid discharged from the impeller trailing edge is ongoing with high rotating speed. But in the ducted pumps, the circumferential velocity is useless. And RGV is commonly installed at downstream to recover this rotating velocity. There are two representative structures. The first type is widely used in boiler water feeding and power plant water circulations, where the stages are cascaded as depicted in Figure 1(a). The RGV blade structure is commonly designed to be cylindrical, as shown in Figures 1(b) and 1(c).

The second type is commonly used in oil drilling and rural and urban water supply from underground deep wells, so it is also called multistage submersible pump or the deep-well pump. As shown in Figure 1(e), the RGV blade structure is twisted like a bowl.

2.1. Structure Analysis. A compact stage for submersible pumps was proposed independently by [34, 35], where the impeller outer diameter is nearly equal to the casing diameter, increasing its stage head. To illustrate the difference between former structure and compact structure, a structure comparison is depicted in Figure 2. Herein, the compact stage means removing the radial diffuser; thus, it can be speculated that there are two extreme cases as depicted in Figures 2(b) and 2(c). For special case I, the impeller diameter D_{21} is not changed, and the casing diameter D_{31} shrinks to D_{32}, and its radial size is greatly reduced. For special case II, the casing diameter D_{31} is not changed, and the impeller diameter D_{21} is increased to D_{22}, and its head is theoretically multiplied by a factor $(D_{22}/D_{21})^2$; thus, less stages are needed and its axial size is shortened. So compact also means saving cost.

On the other hand, the special RGV also is an alternative to the bowl-shaped RGV from the cost saving aspect. But this is beyond our current research and would be regarded in the future.

2.2. Compact Stage Design. To extract oil or water from deep wells, the pump structure must be carefully tailored to utilize the limited space in well bore. In our early work [35], a compact deep-well pump was developed, as shown in Figure 3.

This pump has only three stages, but it's performance exceeds the former multistage pump with five stages. To promote its popularity and to replace former multistage pumps, it is essential to establish a set of mature design procedures, especially for RGV. Though such efforts as steady-state simulation and experimental testing have been conducted to improve its hydraulic performance, cylindrical blade shape generally impedes through flow performance of RGV [36–39], as well as its pressure recovery. This point can be demonstrated by the principles of centrifugal pumps [40], where flow angles are varied along the leading edge to reduce the incidence loss. Therefore, a new circumferential twisted guide vane is proposed to tackle this problem.

3. A New RGV Structure

3.1. Twisted Blade Design Principle. A new RGV structure is developed by three streamlines at different spanwise position. As shown in Figure 4(a), by fixing the top streamline *c*, extending the mid span streamline *b* along the circumferential direction and further extending the bottom streamline *a* forward, a triple-streamline surface is constructed, where the three streamlines are drawn by our in-house code NQSJ [41], which is a general purpose RGV profile design tool. Then by cutting off the triangle block *ABC* from the round plate, a channel passage is formed, as shown in Figure 4(a).

Further, as shown in Figure 4(b), the blade is combined by two joined parts: a cylindrical part *GHIJ* and a twisted part *DEFGH*. Then, a practical RGV is formed as shown in Figure 4(c). Therefore, the key point is to establish the three streamlines *a*, *b*, *c* and the dividing point *G*, which will be discussed hereafter.

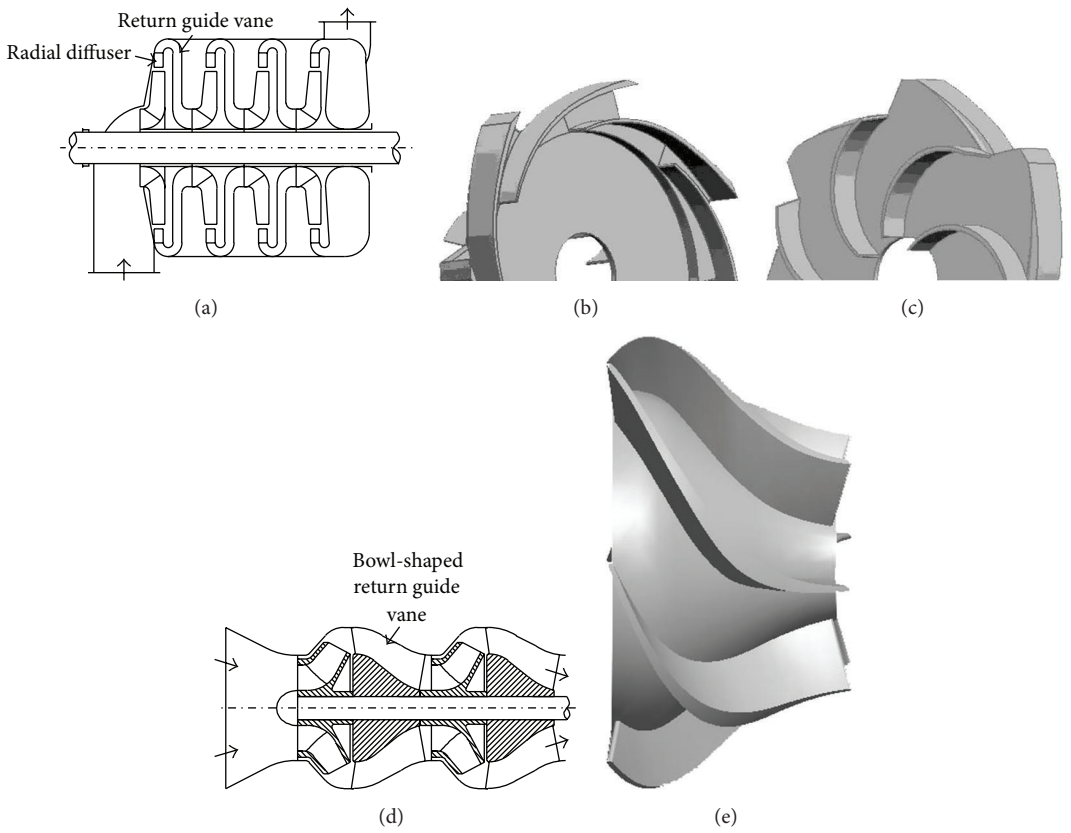

Figure 1: Two multistage pumps: (a) multistage pump equipped with radial diffuser and RGV, (b) radial diffuser, (c) RGV, (d) multistage pump equipped with bowl-shaped RGV, and (e) bowl-shaped RGV.

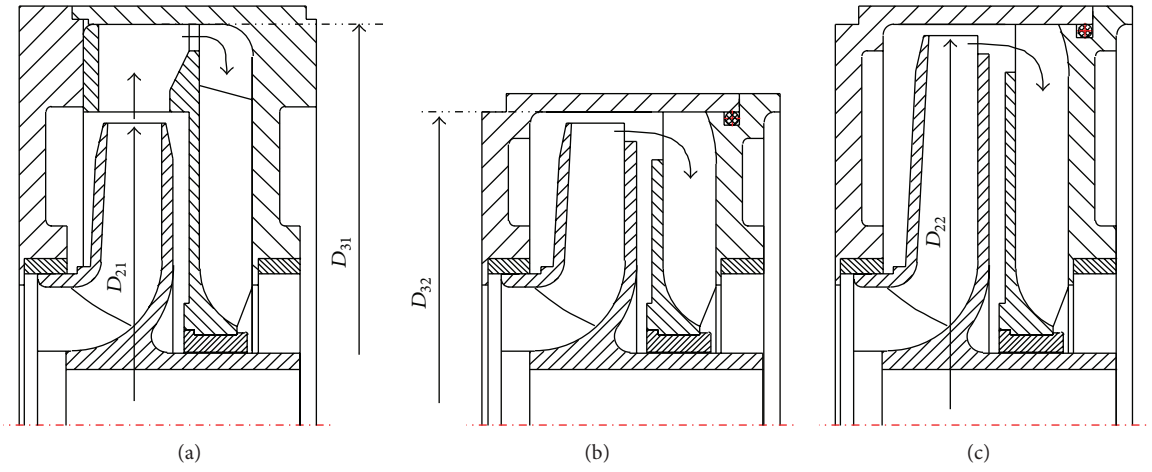

Figure 2: Structure comparison: (a) former structure, (b) special case I, and (c) special case II.

3.2. Twisted Blade Design Procedure. Herein, it is assumed that the impeller design has been finished. And our major concern is the geometric structure of the impeller discharge. To meet design flow rate, the impeller must be cut at the outer edge to achieve enough flow area. As shown in Figure 5, there are two cutting proposals. The first proposal cuts the blade as well as its hub plate, and the second proposal keeps the blade and cuts its hub plate.

Thus, for the first cutting proposal, the effective diameter of impeller is the mean value of the shroud and the hub, $D_2 = (D_{21} + D_{20})/2$, as depicted in Figure 5(a). And the effective diameter for the second proposal is the shroud diameter,

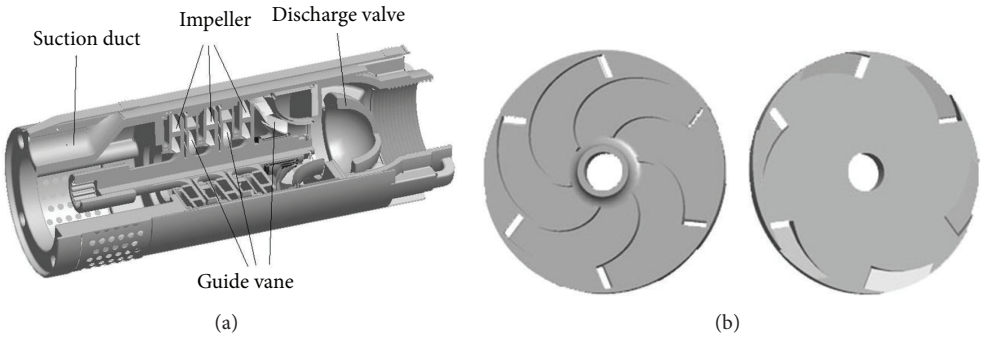

Figure 3: A multistage pump with compact stages: (a) assembly and (b) RGV.

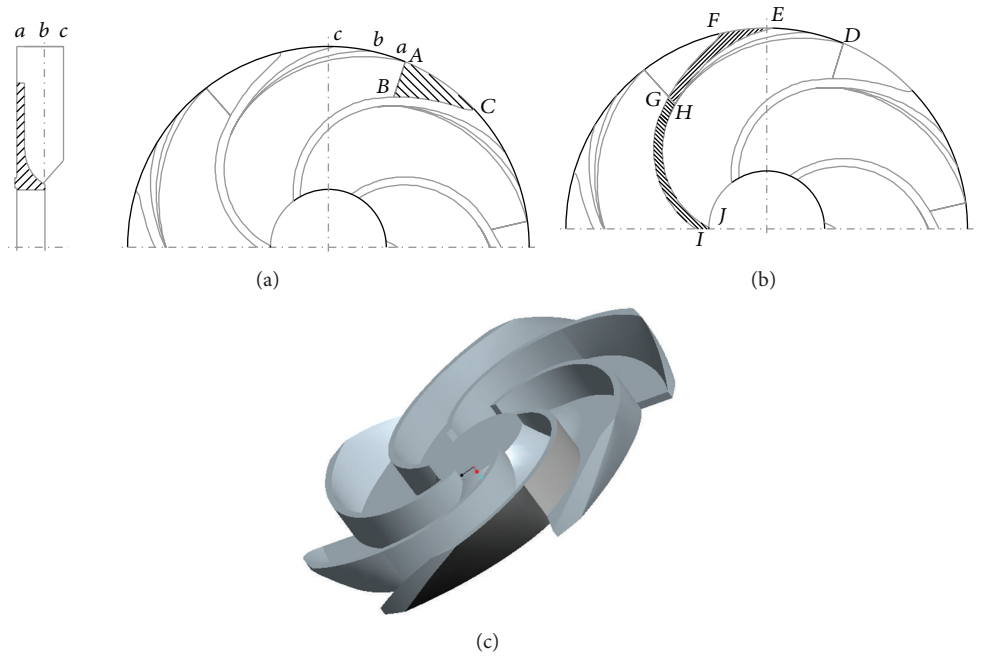

Figure 4: Blade design procedure: (a) schematic of a new RGV, (b) two parts of RGV, and (c) 3D view.

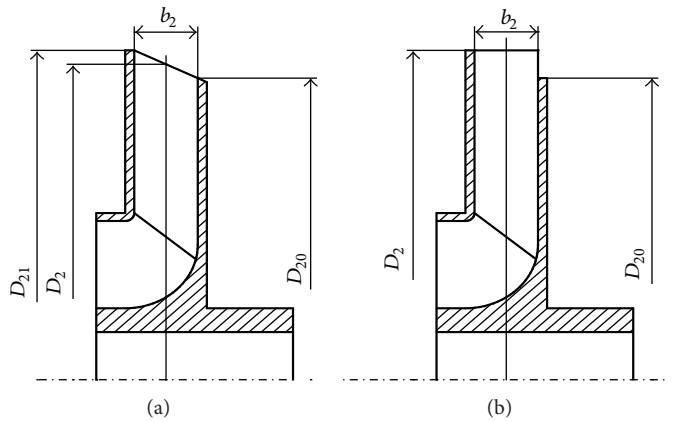

Figure 5: Two cutting proposals: (a) cutting blade outer edge and hub plate and (b) keeping blade and cutting hub plate.

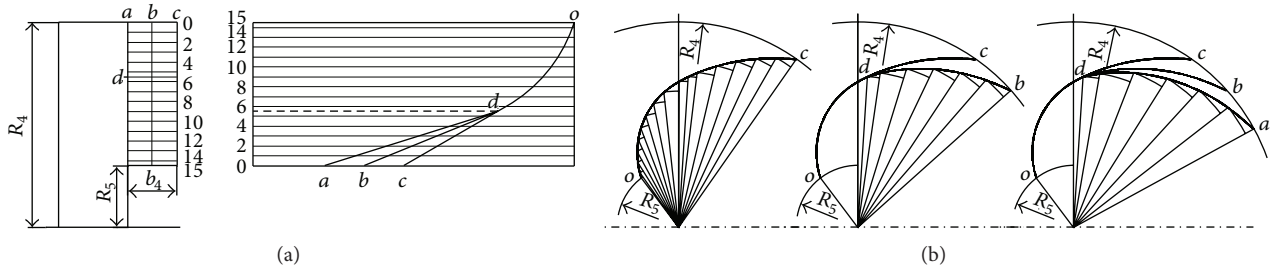

Figure 6: Blade profile drawing procedure: (a) blade angle distribution profiles and (b) blade profiles.

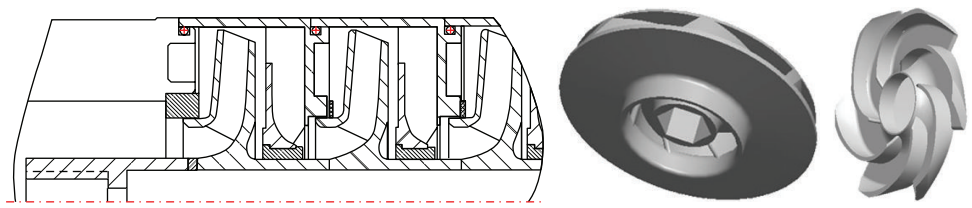

Figure 7: Schematic of 125QSJ10 and its impeller and RGV.

as shown in Figure 5(b). Then, the outer diameter of RGV is $D_4 \in [1.03, 1.08]D_2$. And the inlet meridional velocity at leading edge of RGV is

$$v_{m3} = \frac{4Q}{\pi\left(D_2{}^2 - D_{20}{}^2\right)}. \tag{1}$$

And the circumferential velocity at leading edge of RGV is

$$v_{u3} = \frac{gH/\eta_h}{u_2}, \tag{2}$$

where η_h is the impeller hydraulic efficiency, which is assumed to be known. Thus, with the meridional velocity v_{m3} and circumferential velocity v_{u3}, the RGV inlet flow angle at the streamline a is

$$\alpha_{3a} = \arctan\left(\frac{v_{m3}}{v_{u3}}\right). \tag{3}$$

With circumferential velocity decreasing, the inlet flow angle at streamline b and c is increased gradually. As the flow field information within RGV is insufficient, it is presumed that $\alpha_{3b} = \alpha_{3a}+$ const, and $\alpha_{3c} = \alpha_{3b}+$ const, where the const can be revised at design stage. Similarly, the RGV outlet angle is presumed to be at $\alpha_4 \in [45^\circ, 90^\circ]$, the wrap angle is at $\phi \in [60^\circ, 130^\circ]$, and the RGV blade height $b_4 \in [1.05, 1.4]b_2$. These parameters are flexible at design stage, which can be adjusted via the GUI of our in-house code NQSJ [41]. With these structural parameters, it is ready to draw the blade profile.

The profile drawing procedure is similar to the design of impeller blades [40]. Firstly, the blade angle distribution profile from inlet angle α_3 to outlet angle α_4 is constructed by a Bezier curve as plotted in Figure 6(a), where a, b, c represent the blade angle distribution profile of three streamlines and d represents the dividing point. And the cubic Bezier curve is

$$\begin{aligned}\mathrm{Bez}(s) = {} & P_0(1-s)^3 + 3P_1 s(1-s)^2 \\ & + 3P_2 s^2(1-s) + P_3 s^3, \quad s \in [0,1],\end{aligned} \tag{4}$$

where P_0 represents the inlet point, that is, points a, b, and c, and P_3 represents the outlet point, that is, point o, as shown in Figure 6(a). P_1 and P_2 are auxiliary points which are controlled by NQSJ. With the angle distribution profiles, the corresponding blade profiles are plotted point by point as shown in Figure 6(b).

Table 1: Design parameters of impeller.

Q (m^3/h)	H (m)	n (r/min)	Z_I	D_{21} (mm)	D_{20} (mm)	b_2 (mm)
10	8.5	2850	7	103	98	8

Table 2: Design parameters of RGV.

Z_R	D_4 (mm)	B_4 (mm)	α_{3a} (°)	α_{3b} (°)	α_{3c} (°)	α_4 (°)	ϕ (°)
6	105	10	10	13.5	16.5	65	75

4. Instantaneous Rotor-Stator Interaction Analysis

4.1. Pump Configurations. To examine the new RGV design method, a prototype pump 125QSJ10 is designed, which means the pump is used in a 125 mm (4 inch) deep well. The impeller discharge is cut using the first proposal. The major design parameters are listed in Tables 1 and 2.

To shorten design cycle, a hydraulic design system NQSJ [40] is heavily used in the blade design and optimization procedures. And the main structure and such hydraulic components as impeller and RGV are depicted in Figure 7.

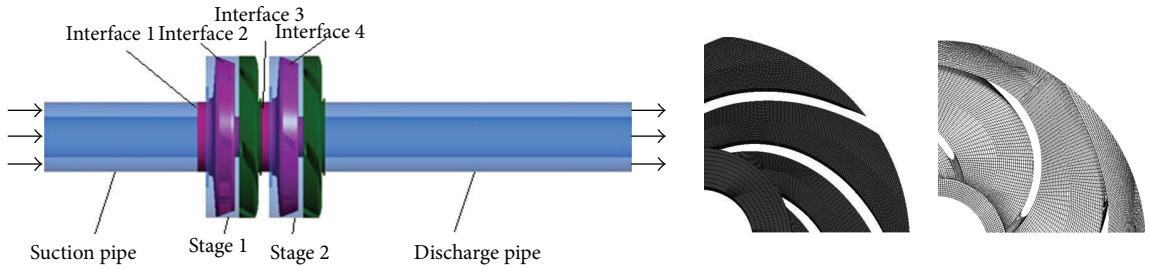

Figure 8: Dual-stage calculation model and numerical grids.

4.2. Numerical Configuration

4.2.1. Basic Equations. For incompressible flows, mass conservation equation is

$$\frac{\partial \rho}{\partial t} + \nabla \cdot (\rho \mathbf{u}) = 0. \tag{5}$$

For flows under noninertial rotating frame, momentum conservation equation is

$$\begin{aligned} \frac{\partial (\rho \mathbf{u})}{\partial t} + \nabla \cdot (\rho u \mathbf{u}) + \rho \left[2\boldsymbol{\omega} \times \mathbf{u} + \boldsymbol{\omega} \times \boldsymbol{\omega} \times \mathbf{r}\right] \\ = -\nabla p + \nabla \cdot \sigma, \end{aligned} \tag{6}$$

where $\boldsymbol{\sigma} = \mu(\partial v_i/\partial x_j + \partial v_j/\partial x_i)$, $2\boldsymbol{\omega} \times \mathbf{u}$ represents the Coriolis force and $\boldsymbol{\omega} \times \boldsymbol{\omega} \times \mathbf{r}$ represents centrifugal force. And the previous equations applies for the multistage centrifugal pumps.

The RNG k-ε model is used for treatment of turbulence:

$$\begin{aligned} \frac{\partial k}{\partial t} + u_i \frac{\partial k}{\partial x_i} &= \frac{\partial}{\partial x_j}\left[\alpha_k \frac{\mu_{\text{eff}}}{\rho} \frac{\partial k}{\partial x_j}\right] \\ &\quad + \frac{\mu_t}{\rho}\left[\frac{\partial u_i}{\partial x_j} + \frac{\partial u_j}{\partial x_i}\right]\frac{\partial u_i}{\partial x_j} - \varepsilon, \\ \frac{\partial \varepsilon}{\partial t} + u_i \frac{\partial \varepsilon}{\partial x_i} &= \frac{\partial}{\partial x_j}\left[\alpha_\varepsilon \frac{\mu_{\text{eff}}}{\rho} \frac{\partial \varepsilon}{\partial x_j}\right] \\ &\quad + C_{1\varepsilon}\frac{\varepsilon}{k}\frac{\mu_t}{\rho}\left[\frac{\partial u_i}{\partial x_j} + \frac{\partial u_j}{\partial x_i}\right]\frac{\partial u_i}{\partial x_j} - C^*_{2\varepsilon}\frac{\varepsilon^2}{k}, \\ C^*_{2\varepsilon} &= C_{2\varepsilon} + \frac{C_\mu \eta^3 (1 - \eta/\eta_0)}{1 + \beta\eta^3}, \end{aligned} \tag{7}$$

where $\mu_{\text{eff}} = \mu + \mu_t$ represents effective viscosity, and $\mu_t = \rho C_\mu (k^2/\varepsilon)$ represents turbulent viscosity. And $\eta = [2S_{ij} \cdot S_{ij}]^{1/2}(k/\varepsilon)$, where $S_{ij} = (1/2)[\partial u_i/\partial x_j + \partial u_j/\partial x_i]$ is fluid strain rate. And the model related constants are $C_\mu = 0.0845$, $\alpha_k = \alpha_\varepsilon = 1.393$, $C_{1\varepsilon} = 1.42$, $C_{2\varepsilon} = 1.68$, $\eta_0 = 4.38$, and $\beta = 0.012$. To date, a better choice of turbulence model for rotating flow within turbomachines is still not available. Relatively, the application of RNG k-ε model receives more support, as well as its accuracy.

Table 3

Number of cells	Stage head (m)	Error (%)
700,584	10.173	5.08
1,300,745	9.982	2.907
1,510,374	9.958	2.66

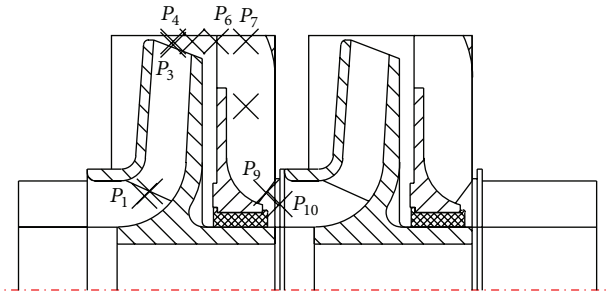

Figure 9: Pressure monitoring positions.

4.2.2. CFD Setup. The calculation model is set up in the commercial package Ansys FLUENT to perform the simulation. A dual-stage calculation model is built to evaluate its performance. And there are four sets of interfaces between the stationary parts and the rotating parts, as shown in Figure 8.

The mean velocity inlet boundary condition is prescribed on the suction, where the velocity is $U_{\text{suc}} = 4Q/\pi({D_1}^2 - {D_h}^2)$, D_1 is the impeller suction diameter, and D_h is the impeller hub diameter. And the flow at discharge is supposed to be fully developed, so the Neumann boundary condition $\partial\varphi/\partial n = 0$ is imposed, φ represents such unknown variables as velocity, pressure, and turbulence scalars. No-slip boundary condition is imposed on the impeller and the guide vane wall boundaries, where $\varphi = 0$. And the turbulent flows are simulated by the RNG k-ε model and the wall function for near wall treatment.

4.2.3. Grid Irrelevance Analysis. The numerical mesh was generated by Ansys ICEM, where yplus $\in [30, 150]$. Then, the steady-state simulation is performed to achieve such

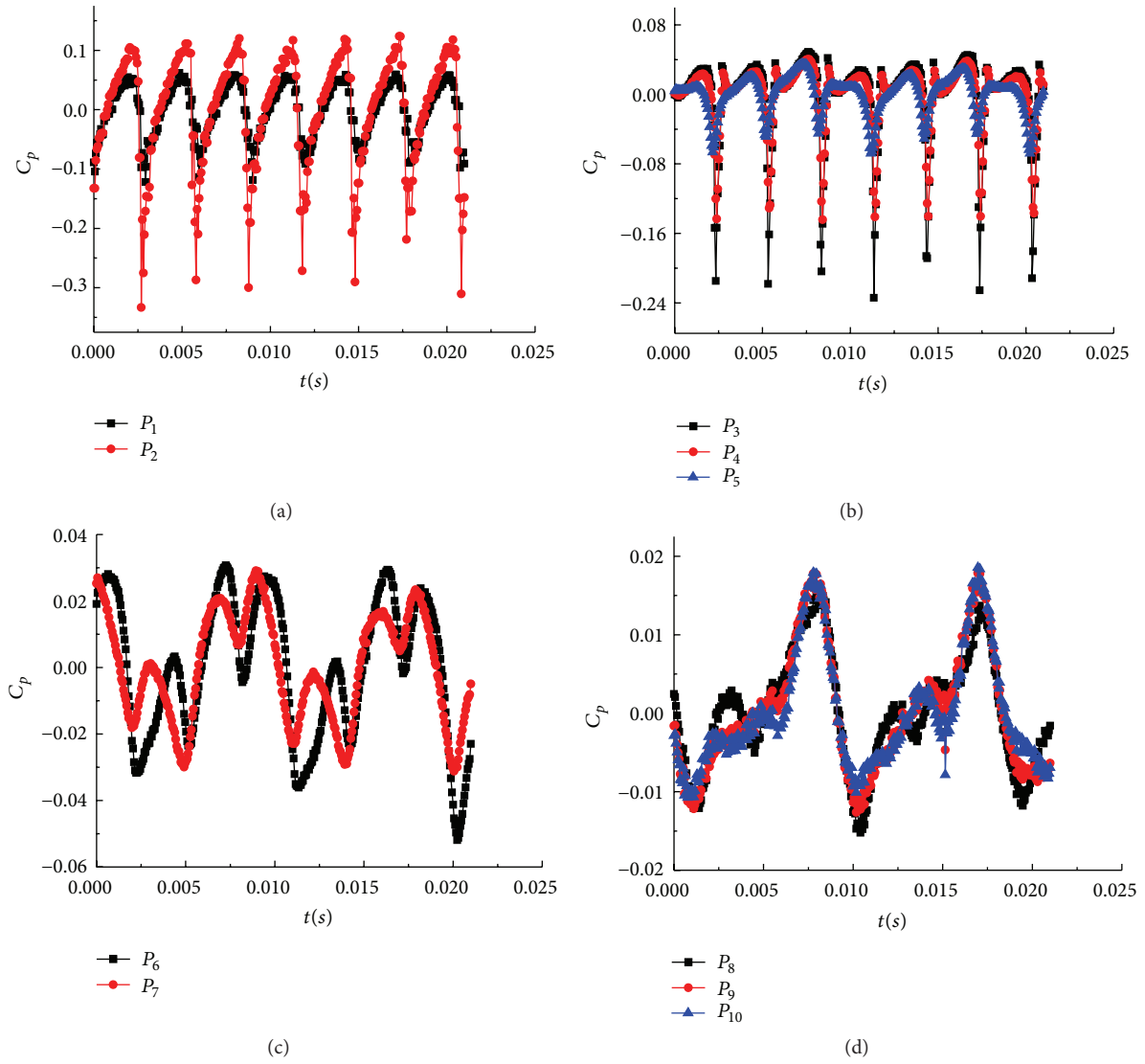

FIGURE 10: Pressure fluctuation at different locations: (a) impeller leading edge, (b) impeller trailing edge, (c) RGV leading edge, and (d) within RGV.

time-averaged characteristics as pump head, torque and efficiency. The stage head is

$$H = \frac{\left(P_{\text{tot}_{\text{dis}}} - P_{\text{tot}_{\text{suc}}}\right)}{\rho g}, \tag{8}$$

where $P_{\text{tot}_{\text{dis}}}$ represents the stage total pressure at discharge and $P_{\text{tot}_{\text{suc}}}$ represents the stage total pressure at suction. And the stage efficiency is

$$\text{Eff} = \frac{\rho g H Q}{M\omega}. \tag{9}$$

With steady-state simulations, the grid irrelevance is examined at three grid levels. And the obtained stage head and its estimated error are listed in Table 3.

So in the present study, the magnitude of mesh size is around 1,500,000; thus, the grid irrelevance can be guaranteed.

4.3. Rotor-Stator Interaction. Instantaneous rotor-stator interaction rather than steady-state flow field reveals the real-time flow situation. Herein, the sliding mesh is used for the rotor-stator interaction analysis. And the pressure coefficient is used to evaluate its fluctuation as follows:

$$C_p = \frac{p - \overline{p}}{\rho u_2{}^2/2}, \tag{10}$$

where $\overline{p}$ is the averaged pressure within a rotation and u_2 is the impeller wheel velocity.

As shown in Figure 9, pressure monitorings are conducted at ten different positions within the impeller and RGV.

In Figures 10(a) and 10(b), with blade perturbation, the pressure fluctuation is formed within the impeller. It is cyclic symmetric at the leading edge. Inherently, the fluctuation runs seven peaks and valleys, equaling to the number of blades. And gradually, it is deviated from the cyclic symmetry

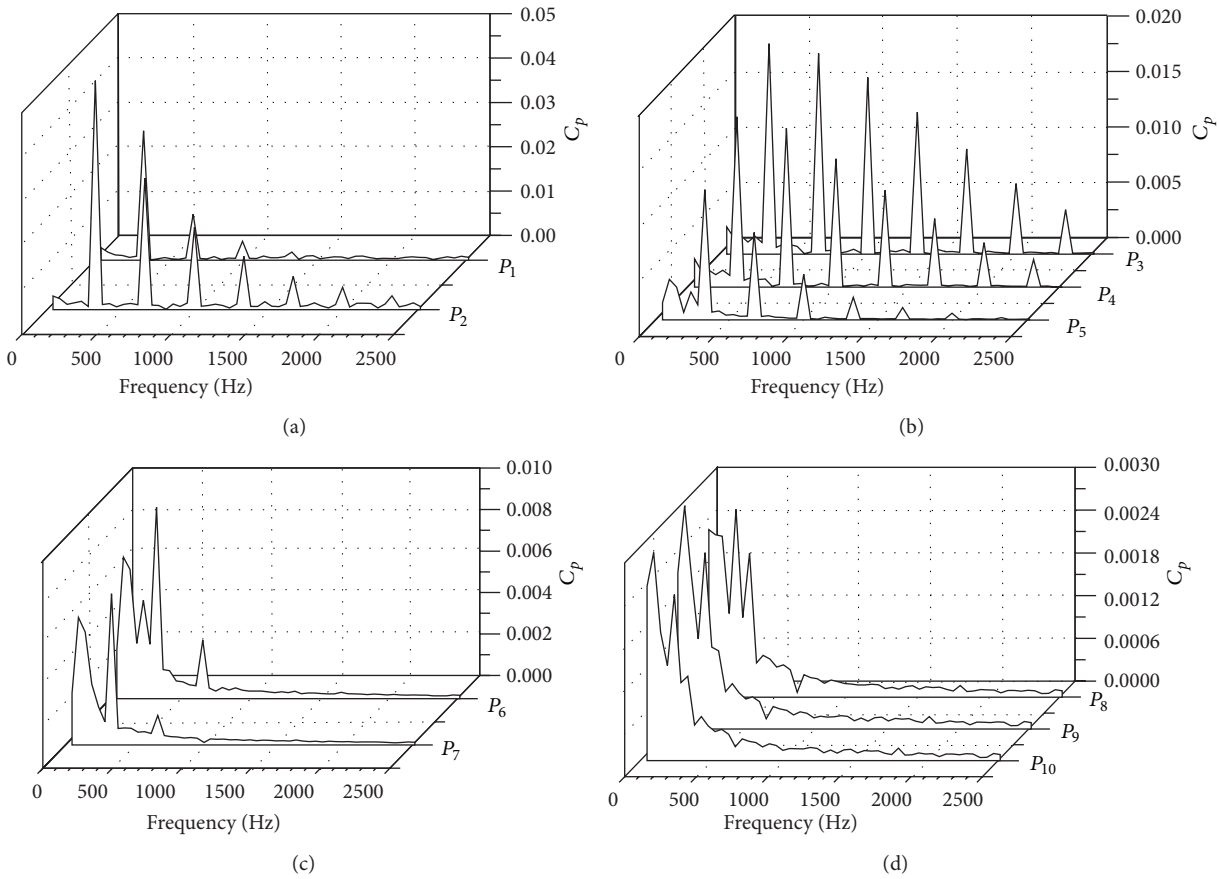

Figure 11: Frequency spectra at different locations: (a) impeller leading edge, (b) impeller trailing edge, (c) RGV leading edge, and (d) within RGV.

by the intervention of RGV. With water outflowing from impeller, the fluctuation appears to be abnormal, as shown in Figure 10(c). But with the renormalization of RGV, it reappears cyclic, but only two peaks and valleys are retained as shown in Figure 10(d).

The frequency spectra are shown in Figure 11, which are obtained by FFT transformations. For multistage pumps, the impeller frequency is

$$f_I = \frac{nZ_I}{60}. \tag{11}$$

Substitute $n = 2850$ (r/min), $Z_I = 7$, into (10), f_I is 332.5 Hz. In impeller, as above the fluctuation frequency is dominated by the impeller frequency, that is, 332.5 Hz, as shown in Figures 11(a) and 11(b). With water outflowing from the impeller, the impeller frequency is even pronounced, but a secondary frequency appears with magnitude $n/60$, that is, 47.5 Hz, which is the rotation frequency, as shown in Figure 11(c). Within RGV, the rotation frequency dominates, and the impeller frequency becomes the secondary frequency, as shown in Figure 11(d).

4.4. Prototype Pump Testing. To verify the previous design strategies, a four-stage pump is designed and tested. The testing is conducted at the pump test rig of the Fujian Academy of Mechanical Sciences. And the stage-averaged performance, such as the flow rate versus head and the flow rate versus efficiency curves are plotted in Figure 12.

In Figure 12, the results show that the peak efficiency is 57.5%, and the stage head is 9 m. And its efficiency is comparable to former multistage pumps, while commonly the stage head of former multistage pump is near 6.5 m. So the more head is needed, the greater cost-saving potential it will produce.

5. Conclusions

In this study, a compact structure is put forward and compared with the former structure of multistage centrifugal pumps. It is evident that its light weight and mobility will attract more prospective users. To meet this compact structure, a new RGV design is proposed. By using a triple-streamline surface shaping, a circumferential twisted RGV is developed.

To validate this design, the instantaneous rotor-stator interactions are investigated using the sliding mesh. And the pressure fluctuations are analyzed. The results show that the maximum fluctuation appears at the leading edge of RGV. And at the trailing edge of RGV the fluctuation is almost negligible. To check validity of this design, a prototype

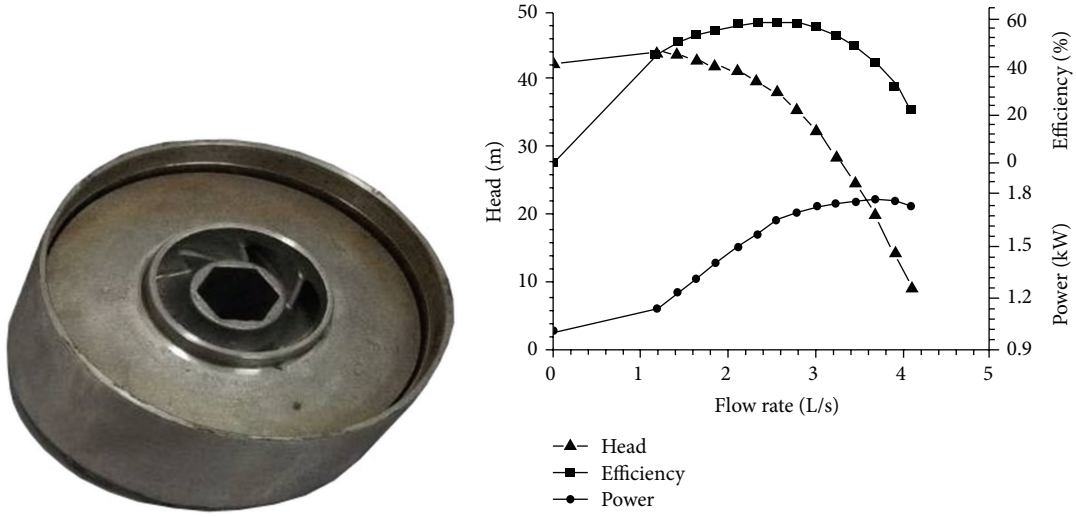

Figure 12: Prototype pump and its characteristic curves.

pump 125QSJ10 is developed and its characteristic curves are obtained. And its performance is comparable with the former multistage pump. But under a given downhole installation diameter, the compact structure with four stages can replace the former pump with six stages, clarifying its superiority.

On the other hand, in many areas where water resource is lacking, such as desert areas and arid areas, pumping water from underground is very inefficient with traditional reciprocating pumps, as well as in many oil-drilling applications; the new design would be an efficient alternative to reducing energy consumptions. Evidently, this compact multistage pump with new RGV is cost saving, which is attractive for the users.

Nomenclature

b_2: Impeller discharge width
b_4: RGV width
D_1: Impeller suction diameter
D_2: Impeller discharge diameter
D_4: RGV inlet diameter
D_h: Impeller hub diameter
f: Frequency
g: Acceleration of gravity
H: Stage head
k: Turbulent energy
M: Angular momentum
n: Rotating speed
p: Pressure
$\mathbf{r}$: Radius vector
S: Fluid strain rate tensor
t: Time
$\mathbf{u}$: Relative velocity vector
V: Inlet velocity
v_{u3}: Circumferential velocity at leading edge of RGV
v_{m3}: Meridional velocity at leading edge of RGV
Z: Blade number
α: Blade angle of RGV
ε: Dissipate rate
η: Hydraulic efficiency
μ: Fluid dynamic viscosity
ρ: Fluid density
$\boldsymbol{\sigma}$: Fluid stress tensor
φ: Unknown variable
ϕ: Wrap angle of RGV
$\boldsymbol{\omega}$: Angular velocity vector.

Superscripts

$\bar{}$: For average.

Subscripts

a: Streamline a
b: Streamline b
c: Streamline c
dis: Discharge of stage
eff: Effective
h: Hydraulic
i, j: Index, that is, 1, 2, 3
I: Impeller
R: RGV
Suc: Suction of stage.

Acknowledgments

The authors would like to acknowledge the supports received from the National Natural Science Foundation of China (Grants No. 51079063 and No. 51109093), the Scientific Research Foundation for Senior Talents of Jiangsu University (No. 11JDG085), the Postdoctoral foundation of Jiangsu Province (No. 1102157C), the Postdoctoral Science foundation

of China (No. 2013M531282), and the National Key Technology R&D Program of the Ministry of Science and Technology of China (No. 2011BAF14B01).

References

[1] A. Thakker, T. S. Dhanasekaran, and J. Ryan, "Experimental studies on effect of guide vane shape on performance of impulse turbine for wave energy conversion," *Renewable Energy*, vol. 30, no. 15, pp. 2203–2219, 2003.

[2] A. Thakker and T. S. Dhanasekaran, "Computed effect of guide vane shape on performance of impulse turbine for wave energy conversion," *International Journal of Energy Research*, vol. 29, no. 13, pp. 1245–1260, 2005.

[3] L. M. C. Ferro, L. M. C. Gato, and A. F. O. Falcão, "Design and experimental validation of the inlet guide vane system of a mini hydraulic bulb-turbine," *Renewable Energy*, vol. 35, no. 9, pp. 1920–1928, 2010.

[4] M. Govardhan and T. S. Dhanasekaran, "Effect of guide vanes on the performance of a self-rectifying air turbine with constant and variable chord rotors," *Renewable Energy*, vol. 26, no. 2, pp. 201–219, 2002.

[5] Q. Li, H. Quan, R. Li, and D. Jiang, "Influences of guide vanes airfoil on hydraulic turbine runner performance," in *Proceedings of the International Conference on Modern Hydraulic Engineering (CMHE '12)*, pp. 703–708, Nanjing, China, March 2012.

[6] A. Mohseni, E. Goldhahn, R. A. Van den Braembussche, and J. R. Seume, "Novel IGV designs for centrifugal compressors and their interaction with the impeller," *Journal of Turbomachinery*, vol. 134, no. 2, Article ID 021006, 8 pages, 2012.

[7] S. L. Gunter, S. A. Guillot, W. F. Ng, and S. T. Bailie, "A three-dimensional CFD design study of a circulation control inlet guide vane for a transonic compressor," in *Proceedings of the 54th ASME Turbo Expo 2009*, pp. 91–101, Orlando, Fla, USA, June 2009.

[8] M. Hensges, "Simulation and optimization of an adjustable inlet guide vane for industrial turbo compressors," in *Proceedings of the 53rd ASME Turbo Expo 2008*, pp. 11–20, Berlin, Germany, June 2008.

[9] M. Coppinger and E. Swain, "Performance prediction of an industrial centrifugal compressor inlet guide vane system," *Proceedings of the Institution of Mechanical Engineers A*, vol. 214, no. 2, pp. 153–164, 2000.

[10] J. Fukutomi and R. Nakamura, "Performance and internal flow of cross-flow fan with inlet guide vane," *JSME International Journal B*, vol. 48, no. 4, pp. 763–769, 2005.

[11] W. K. Chan, Y. W. Wong, S. C. M. Yu, and L. P. Chua, "A computational study of the effects of inlet guide vanes on the performance of a centrifugal blood pump," *Artificial Organs*, vol. 26, no. 6, pp. 534–542, 2002.

[12] V. Chernoray, S. Ore, and J. Larsson, "Effect of geometry deviations on the aerodynamic performance of an outlet guide vane cascade," in *Proceedings of the ASME Turbo Expo 2010: Power for Land, Sea, and Air*, pp. 381–390, Glasgow, UK, June 2010.

[13] T. Sonoda and H. Schreiber, "Aerodynamic characteristics of supercritical outlet guide vanes at low Reynolds number conditions," *Journal of Turbomachinery*, vol. 129, no. 4, pp. 694–704, 2007.

[14] H. Posson, S. Moreau, and M. Roger, "Broadband noise prediction of fan outlet guide vane using a cascade response function," *Journal of Sound and Vibration*, vol. 330, no. 25, pp. 6153–6183, 2011.

[15] C. Clemen, "Aero-mechanical optimisation of a structural fan outlet guide vane," *Structural and Multidisciplinary Optimization*, vol. 44, no. 1, pp. 125–136, 2011.

[16] A. G. Barker and J. F. Carrotte, "Influence of compressor exit conditions on combustor annular diffusers, part 1: diffuser performance," *Journal of Propulsion and Power*, vol. 17, no. 3, pp. 678–685, 2001.

[17] V. Cyrus and J. Polansky, "Numerical simulation of the flow pulsations origin in cascades of the rear blade rows in a gas turbine axial compressor using low calorific fuel," *Journal of Turbomachinery*, vol. 132, no. 3, Article ID 031012, 11 pages, 2010.

[18] D. Kaya, "Experimental study on regaining the tangential velocity energy of axial flow pump," *Energy Conversion and Management*, vol. 44, no. 11, pp. 1817–1829, 2003.

[19] W. Yan, D. Shi, Z. Luo, and Y. Lu, "Three-dimensional CFD study of liquid-solid flow behaviors in tubular loop polymerization reactors: the effect of guide vane," *Chemical Engineering Science*, vol. 66, no. 18, pp. 4127–4137, 2011.

[20] A. Sulaiman and S. Gabin, "Flow through the return channel of a multistage centrifugal pump," in *Proceedings of the 5th Conference on Fluid Machinery*, vol. 2, pp. 1121–1132, Akademiai Kiado, Budapest, Hungary, 1975.

[21] S. König and N. Petry, "Parker-type acoustic resonances in the return guide vane cascade of a centrifugal compressor—theoretical modeling and experimental verification," in *Proceedings of the ASME Turbo Expo 2010: Power for Land, Sea, and Air*, pp. 1687–1700, Glasgow, UK, June 2010.

[22] M. Miyano, T. Kanemoto, D. Kawashima, A. Wada, T. Hara, and K. Sakoda, "Return vane installed in multistage centrifugal pump," *The International Journal of Fluid Machinery and Systems*, vol. 1, no. 1, pp. 57–63, 2008.

[23] D. Kawashima, T. Kanemoto, K. Sakoda et al., "Matching diffuser vane with return vane installed in multistage centrifugal pump," *The International Journal of Fluid Machinery and Systems*, vol. 1, no. 1, pp. 86–91, 2008.

[24] J. D. Denton, "Some limitations of turbomachinery CFD," in *Proceedings of the ASME Turbo Expo 2010: Power for Land, Sea, and Air*, pp. 1–11, Glasgow, UK, June 2010.

[25] T. Nagahara and Y. Inoue, "Investigation of hydraulic design for high performance multi-stage pump using CFD," in *Proceedings of the ASME Fluids Engineering Division Summer Conference (FEDSM '09)*, pp. 417–424, Vail, Colo, USA, August 2009.

[26] S. Huang, A. A. Mohamad, and K. Nandakumar, "Numerical simulation of unsteady flow in a multistage centrifugal pump using sliding mesh technique," *Progress in Computational Fluid Dynamics*, vol. 10, no. 4, pp. 239–245, 2010.

[27] T. L. Rodgers and M. Cooke, "Rotor-stator devices: the role of shear and the stator," *Chemical Engineering Research and Design*, vol. 90, no. 3, pp. 323–327, 2012.

[28] N. Sengil, "Performance increase in turbomolecular pumps with curved type blades," *Vacuum*, vol. 86, no. 11, pp. 1764–1769, 2012.

[29] T. Chen and S. C. Li, "Numerical investigation of guide-plate induced pressure fluctuations on guide vanes of three gorges turbines," *Journal of Fluids Engineering*, vol. 133, no. 6, Article ID 061101, 10 pages, 2011.

[30] J. Zhang, H. Zhu, C. Yang, Y. Li, and H. Wei, "Multi-objective shape optimization of helico-axial multiphase pump impeller based on NSGA-II and ANN," *Energy Conversion and Management*, vol. 52, no. 1, pp. 538–546, 2009.

[31] D. Kaya, E. A. Yagmur, K. S. Yigit, F. C. Kilic, A. S. Eren, and C. Celik, "Energy efficiency in pumps," *Energy Conversion and Management*, vol. 49, no. 6, pp. 1662–1673, 2008.

[32] S. Sallem, M. Chaabene, and M. B. A. Kamoun, "Optimum energy management of a photovoltaic water pumping system," *Energy Conversion and Management*, vol. 50, no. 11, pp. 2728–2731, 2009.

[33] M. Gölcü, Y. Pancar, and Y. Sekmen, "Energy saving in a deep well pump with splitter blade," *Energy Conversion and Management*, vol. 50, no. 11, pp. 2728–2731, 2009.

[34] H. Roclawski and D.-H. Hellmann, "Rotor-stator-interaction of a radial centrifugal pump stage with minimum stage diameter," in *Proceedings of the 4th WSEAS International Conference on Fluid Mechanics and Aerodynamics*, pp. 301–308, Elounda, Greece, 2006.

[35] W. Shi, Q. Zhang, and W. Lu, "Hydraulic design of new-type deep well pump and its flow calculation," *Journal of Jiangsu University*, vol. 27, no. 6, pp. 528–531, 2006 (Chinese).

[36] H. Roclawski and D.-H. Hellmann, "Numerical simulation of a radial multistage centrifugal pump," in *Proceedings of the 44th AIAA Aerospace Sciences Meeting and Exhibit*, AIAA2006-1428, Elounda, Greece, January 2006.

[37] H. Roclawski, A. Weiten, and D.-H. Hellmann, "Numerical investigation and optimization of a stator for a radial submersible pump stage with minimum stage diameter," in *Proceedings of the ASME Joint U.S.-European Fluids Engineering Division Summer Meeting (FEDSM '06)*, FEDSM2006-98181, pp. 233–243, Miami, Fla, USA, July 2006.

[38] W. Shi, W. Lu, H. Wang, and Q. Li, "Research on the theory and design methods of the new type submerible pump for deep well," in *Proceedings of the ASME Fluids Engineering Division Summer Conference (FEDSM '09)*, pp. 91–97, Vail, Colo, USA, August 2009.

[39] L. Zhou, W. D. Shi, W. G. Lu et al., "Numerical investigations and performance experiments of a deep-well centrifugal pump with different diffusers," *Journal of Fluids Engineering*, vol. 134, no. 7, Article ID 071102, 8 pages, 2012.

[40] J. F. Gulich, *Centrifugal Pumps*, Springer, New York, NY, USA, 2007.

[41] Q. H. Zhang, Y. Xu, W. D. Shi et al., "Research and development on the hydraulic design system of the guide vanes of multistage centrifugal pumps," *Applied Mechanics and Materials*, vol. 197, pp. 24–30, 2012.